# Supplementary information for: Increased abyssal ocean density stratification across the Middle Pleistocene Transition

Nicola C. Thomas, Heather L. Ford, Mervyn Greaves, and David A. Hodell

**Carbonate ion effect**

In validating Mg/Ca-derived deep-water temperature, an additional consideration is the carbonate ion effect and the hypothesis that carbonate ion concentration ($[CO_3^{2-}]$) may influence the partition of Mg in benthic foraminiferal calcite (Elderfield et al., 2006). This hypothesis is borne out of the observation of strong gradients displayed by some trace elements with increasing water depth which indicate either dissolution or a change in the carbonate ion saturation state (Elderfield et al., 2006).

Foraminiferal Mg/Ca ratios are increasingly used as an independent proxy for estimating seawater palaeotemperatures exploiting the temperature dependent partitioning of Mg during calcification (Elderfield et al., 2006, 2010; Greaves, 2008; Mashiotta et al., 1999; Weldeab et al., 2016), whereby higher Mg ion concentrations are incorporated into foraminiferal calcite lattice with increasing seawater temperature (Elderfield et al., 2010; Greaves, 2008; Mashiotta et al., 1999). Because Mg incorporation in biogenic calcite is biologically mediated, species specific empirical calibrations are required to estimate past deep-water palaeotemperatures (Elderfield et al., 2006, 2010; Greaves, 2008). For some benthic species, such as the epifaunal *Cibicidoides wuellerstorfi* (Sosdian and Rosenthal, 2009) palaeotemperature calibrations may be complicated by the influence of $[CO_3^{2-}]$ on Mg partitioning (Elderfield et al., 2006, 2012; Weldeab et al., 2016; Yu and Broecker, Wallace, 2010; Yu and Elderfield, 2008). Notably, *Cibicidoides wuellerstorfi* exhibits weaker Mg/Ca sensitivity to temperature relative to both *Uvigerina* spp. (Elderfield et al., 2006, 2010) and *Globobulimina affinis* (Weldeab et al., 2016). These infaunal benthic foraminifera, *Uvigerina* spp. and *Globobulimina* spp., which are shallow (1–2 cm) and deep (>1–10 cm) dwelling below the sediment-bottom water interface respectively, are buffered from $[CO_3^{2-}]$ (Elderfield et al., 2006; Stirpe et al., 2021) because they form their tests from pore waters in which $\Delta[CO_3^{2-}]$ tends to zero (Elderfield et al., 2006, 2010; Martin and Sayles, 1996), and where $CaCO_3$ saturation is presumed constant (Birner et al., 2016). Whereas recent evidence suggests porewater $\Delta[CO_3^{2-}]$ is spatially and likely temporally variable with greater potential to influence *Uvigerina* spp. Mg/Ca than originally conceived (Weldeab et al., 2016), *Uvigerina* spp. do not appear to be significantly affected by deep-water changes in carbonate chemistry (Elderfield et al., 2010; Stirpe et al., 2021). Furthermore, Mg/Ca measured in *Globobulimina* spp. has a relatively high temperature sensitivity affording a robust means to estimate past deep-water temperatures (Weldeab et al., 2016).

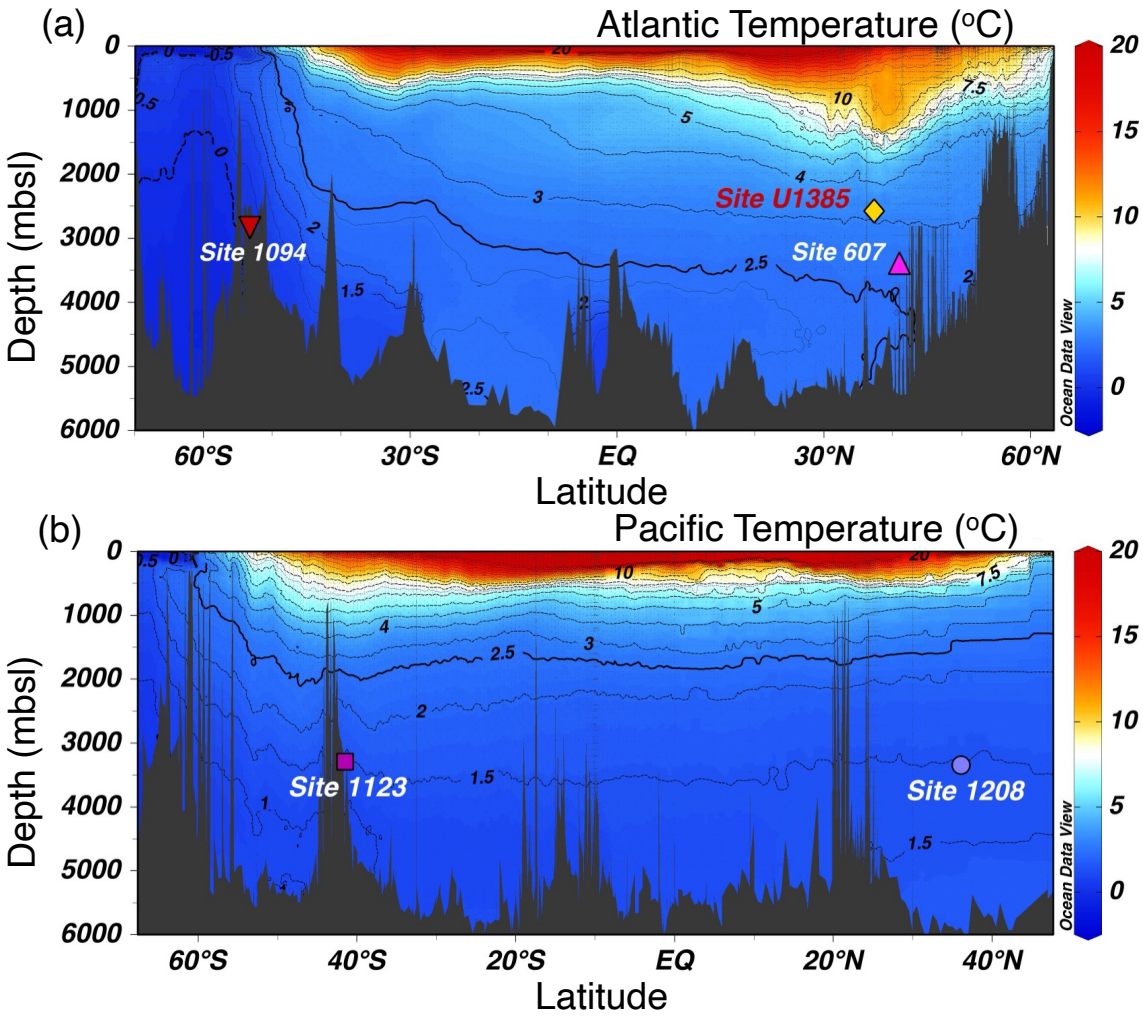


**Figure S1: (a) Atlantic and (b) Pacific meridional hydrographic profiles of deep-water temperature (°C) relative to site locations and depths as in Figure 1.**

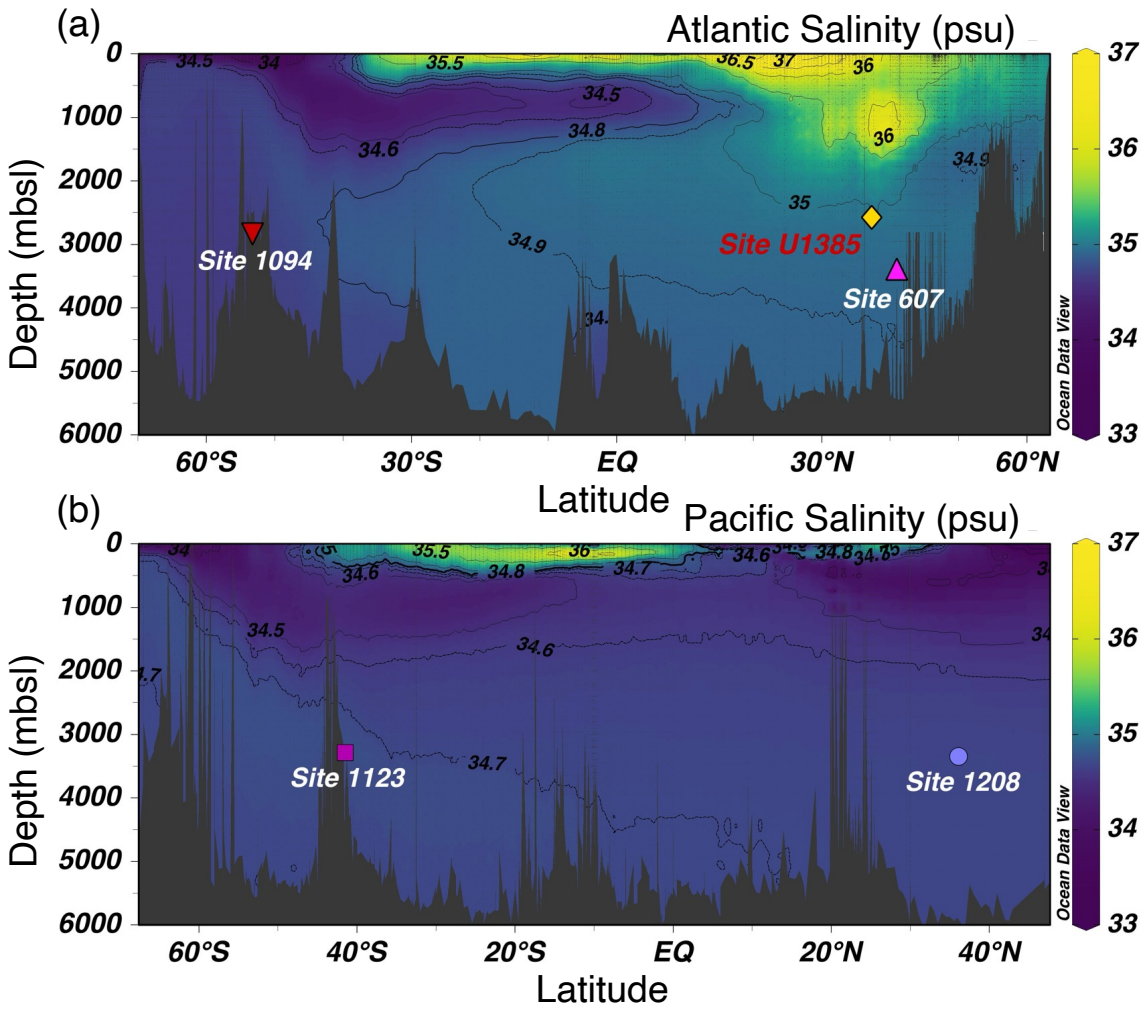


**Figure S2: (a) and (b) respectively Atlantic and Pacific Ocean meridional hydrographic profiles of deep-water salinity showing site locations and depths as in Figure 1.**

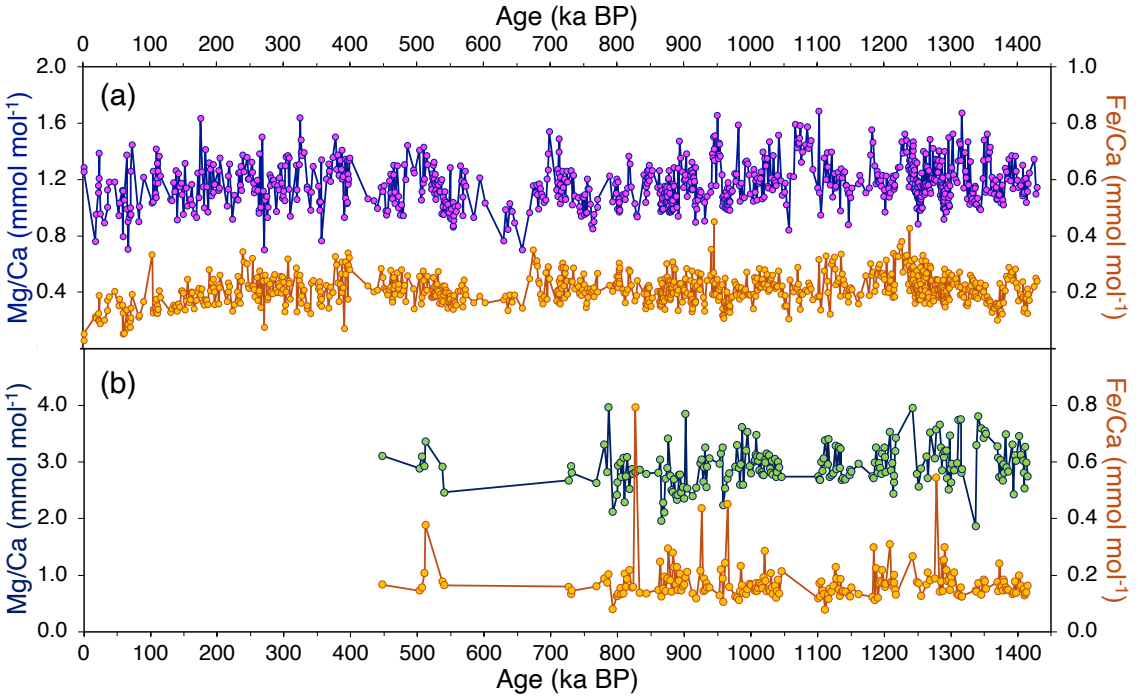


**Figure S3: Site U1385 measured Mg/Ca and Fe/Ca after assessment and removal of co-occurring high values. (a) Comparison of *Uvigerina peregrina* Mg/Ca (dark blue line and pink circles) and Fe/Ca (light brown line with yellow circles). (b) Same as in (a) but with measurements made on *Globobulimina affinis* Mg/Ca (dark blue line and green circles) and Fe/Ca (light brown line with yellow circles). Note the larger scale for *G. affinis* Mg/Ca relative to *U. peregrina*.**

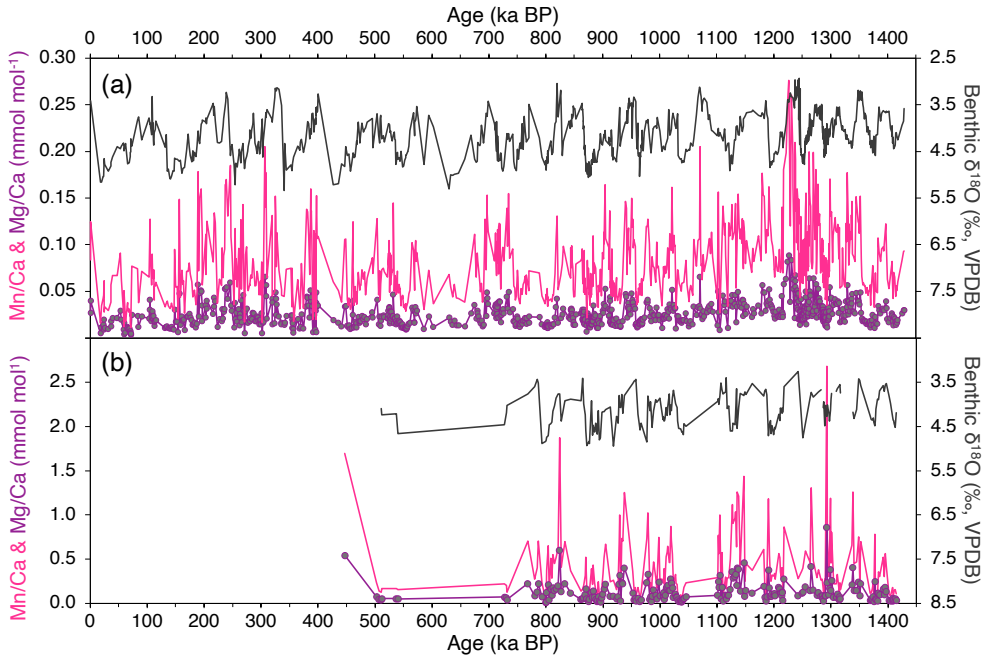


**Figure S4: Downcore glacial-interglacial variations in Site U1385 Mn/Ca. (a) Glacial-interglacial variations depicted by benthic $\delta^{18}O$ (black line); Mn/Ca measured on *Uvigerina peregrina* (pink line) which tends to increase downcore and shows greatest values during interglacials and interstadials with minimum values recorded during glacials; and Mg/Ca correction values (purple line with grey circles) calculated from the Mg/Mn coating correction ratio of 0.32 mol mol$^{-1}$ (Hasenfratz et al., 2017; de Lange et al., 1992) discussed in text. (b) Mn/Ca and Mg/Ca as in (a) measured on *Globobulimina affinis*. Note the larger scale relative to (a).**

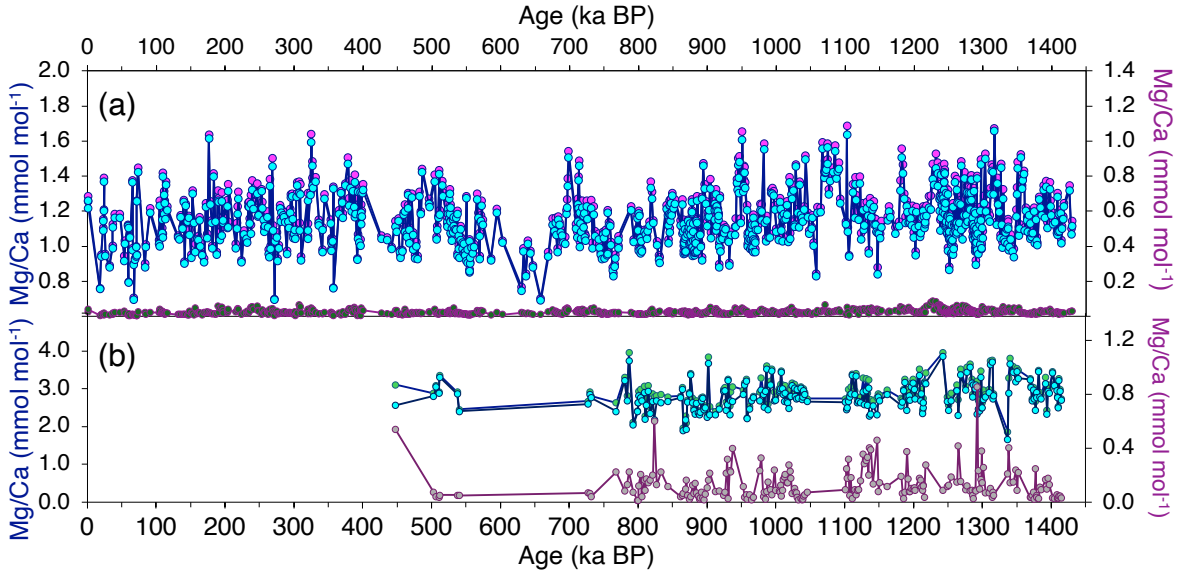


**Figure S5: Mg/Ca data after correction for foraminiferal coating Mg/Mn ratios. (a) *Uvigerina peregrina* measured Mg/Ca (dark blue line with pink circles); Mg/Ca corrected by 0.32 mol mol$^{-1}$ (dark blue line light blue circles); and foraminiferal coating corrections calculated from the Mg/Mn ratio of 0.32 mol mol$^{-1}$ (Hasenfratz et al., 2017; de Lange et al., 1992) (plum with grey circles). (b) The same as in (a) but for *Globobulimina affinis* with green circles instead of pink. Note the larger Mg/Ca scale relative to (a).**

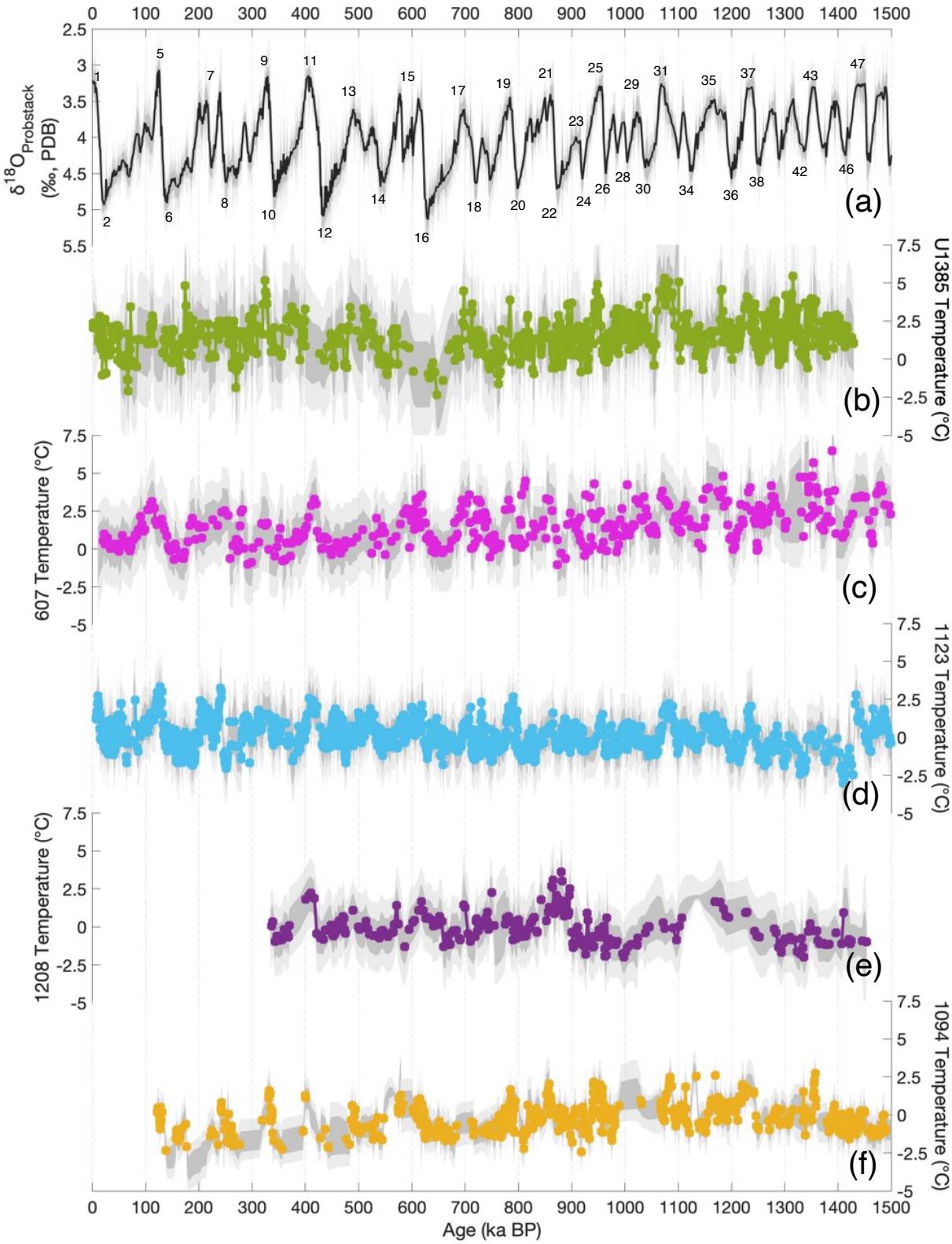


**Figure S6: PSU Solver deep-water Mg/Ca-derived temperature output for all sites. (a) Prob-stack benthic $\delta^{18}O$ (Ahn et al., 2017) (black line) with MIS numbers denoting glacial (even) and interglacial (odd) stages. PSU Solver deep-water Mg/Ca-derived temperature outputs for: (b) IODP Site U1385 (this study and (Birner et al., 2016; Skinner et al., 2003; Skinner and Elderfield, 2007) (green); (c) DSDP Site 607 (Ford et al., 2016; Sosdian and Rosenthal, 2009) (pink); (d) ODP Site 1123 (Elderfield et al., 2012) (blue); (e) ODP Site 1208 (Ford and Raymo, 2020) (purple); and (f) ODP Site 1094 (Hasenfratz et al., 2019) (yellow). Dark and light grey shading represents 1 and 2σ error bars respectively.**

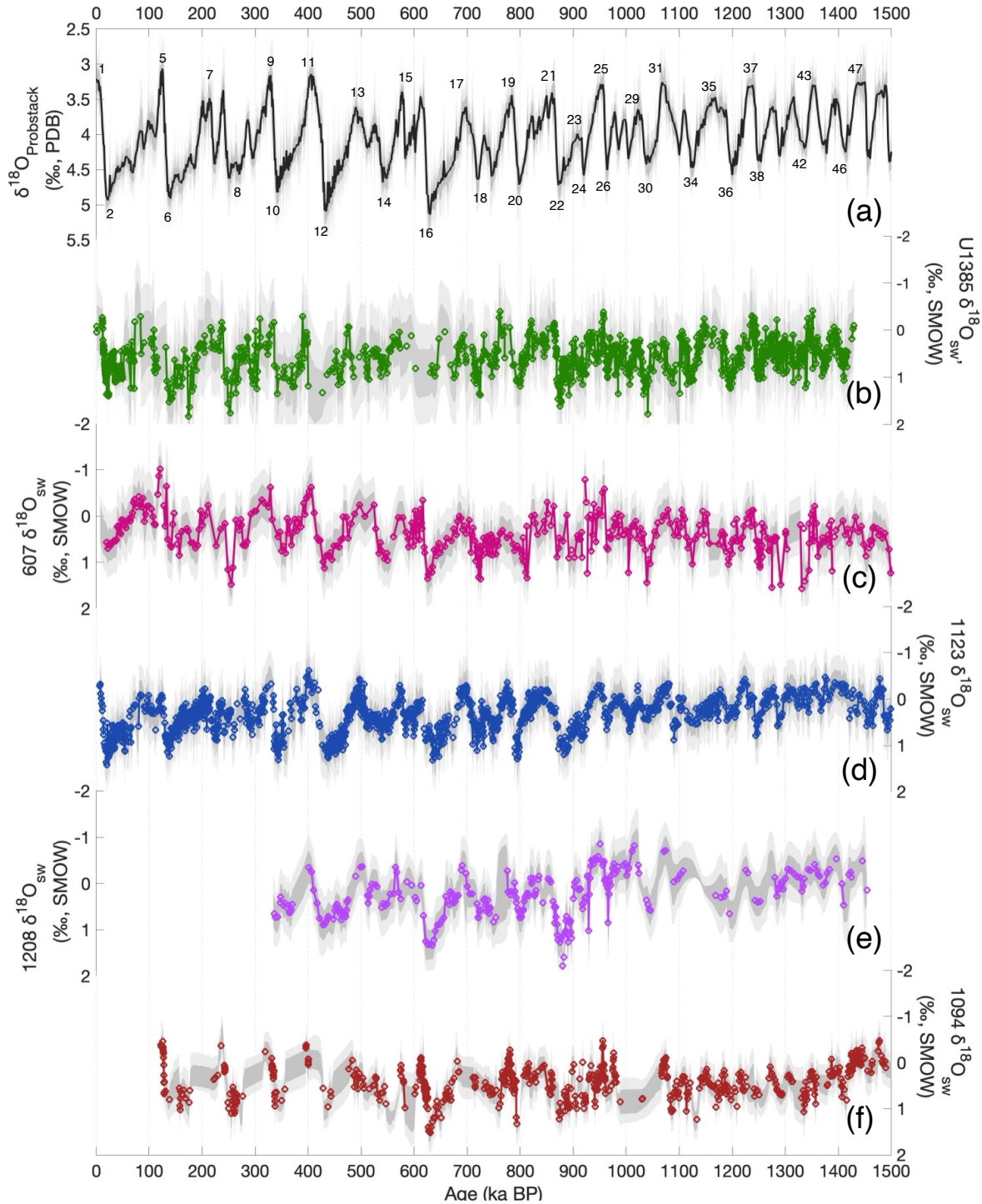


**Figure S7: PSU Solver $\delta^{18}O_{seawater}$ output for all sites. (a) Prob-stack benthic $\delta^{18}O$ (Ahn et al., 2017) (black line) with MIS numbers denoting glacial (even) and interglacial (odd) stages. PSU Solver $\delta^{18}O_{seawater}$ output for: (b) IODP Site U1385 (this study and (Birner et al., 2016; Skinner et al., 2003; Skinner and Elderfield, 2007) dark green); (c) DSDP Site 607 (Ford et al., 2016; Sosdian and Rosenthal, 2009) (dark pink); (d) ODP Site 1123 (Elderfield et al., 2012) (dark blue); (e) ODP Site 1208 (Ford and Raymo, 2020) (purple); and (f) ODP Site 1094 (Hasenfratz et al., 2019) (dark red). Dark and light grey shading represents 1 and 2σ error bars respectively.**

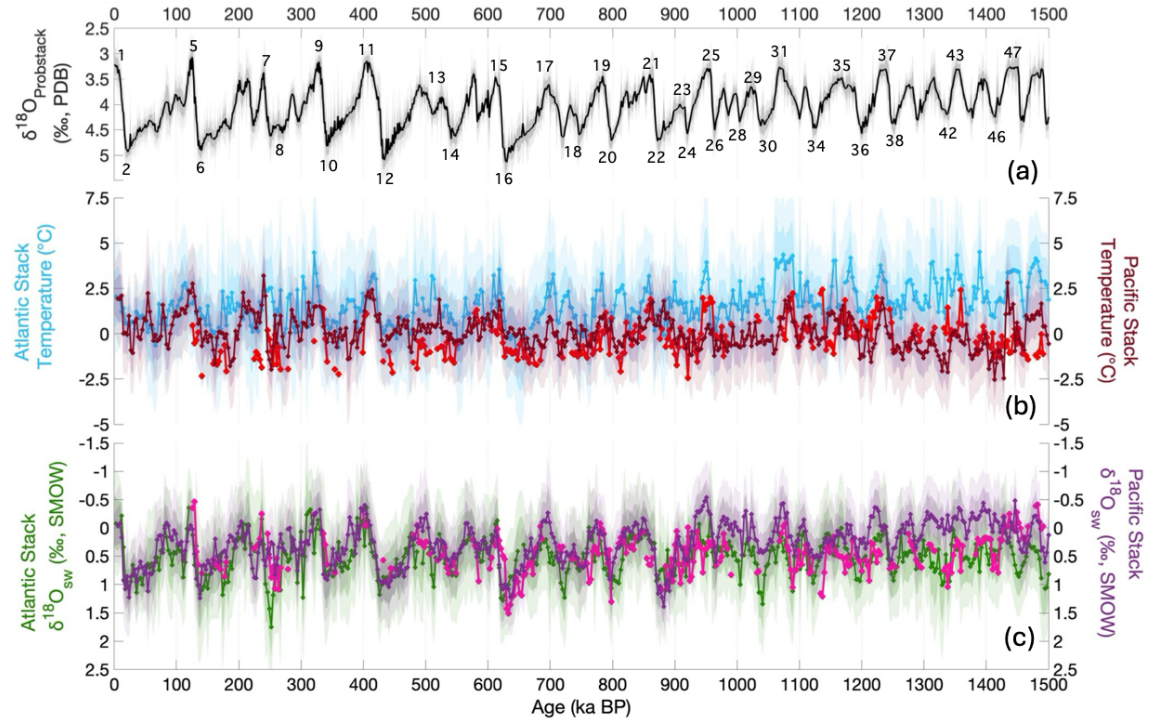


**Figure S8: Comparison of Site 1094 against North Atlantic and Pacific Ocean temperature and benthic $\delta^{18}O_{seawater}$ stacks. (a) Prob-stack benthic $\delta^{18}O$ (Ahn et al., 2017) (black line) MIS numbers denoting glacial stages (below) and interglacials (above). (b) Deep-water temperature stacks for the Pacific Ocean (Elderfield et al., 2012; Ford and Raymo, 2020) (dark red), and the North Atlantic Ocean (this study and (Ford et al., 2016; Sosdian and Rosenthal, 2009) (light blue), overlain by Site 1094 deep-water temperature (Hasenfratz et al., 2019) (bright red). (c) Deep-water $\delta^{18}O_{seawater}$ stacks for the Pacific Ocean (Elderfield et al., 2012; Ford and Raymo, 2020) (dark purple) and the North Atlantic (this study including (Ford et al., 2016; Sosdian and Rosenthal, 2009)) (dark green), overlain by Site 1094 deep-water $\delta^{18}O_{seawater}$ (Hasenfratz et al., 2019) (bright pink) Stacks and their error envelopes represent the means of original manually aligned, interpolated (on 3 kyr interval) and bootstrapped records.**

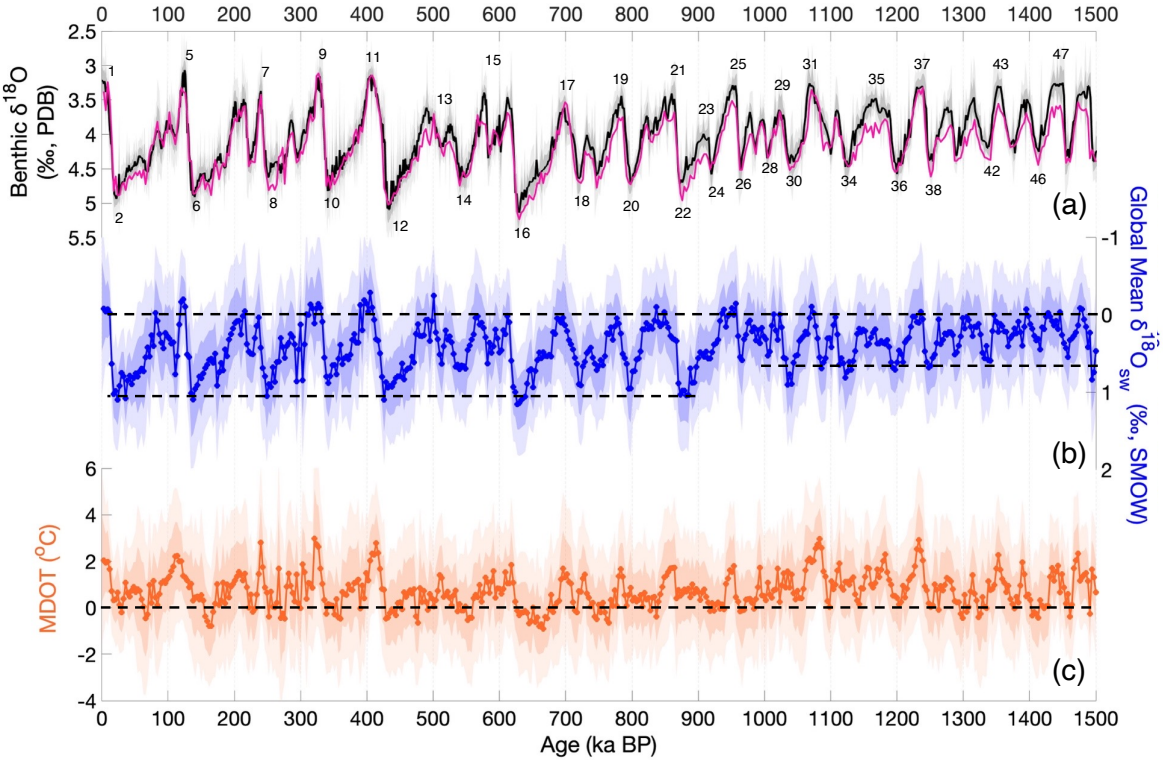


**Figure S9: Non-weighted global mean stacks. Caption as in Figure. 9 but for global benthic $\delta^{18}O$ (a), mean deep-water $\delta^{18}O_{seawater}$ (b) and MDOT (c). Also shown in (a) is the Prob-stack benthic $\delta^{18}O$ (Ahn et al., 2017) (black line).**

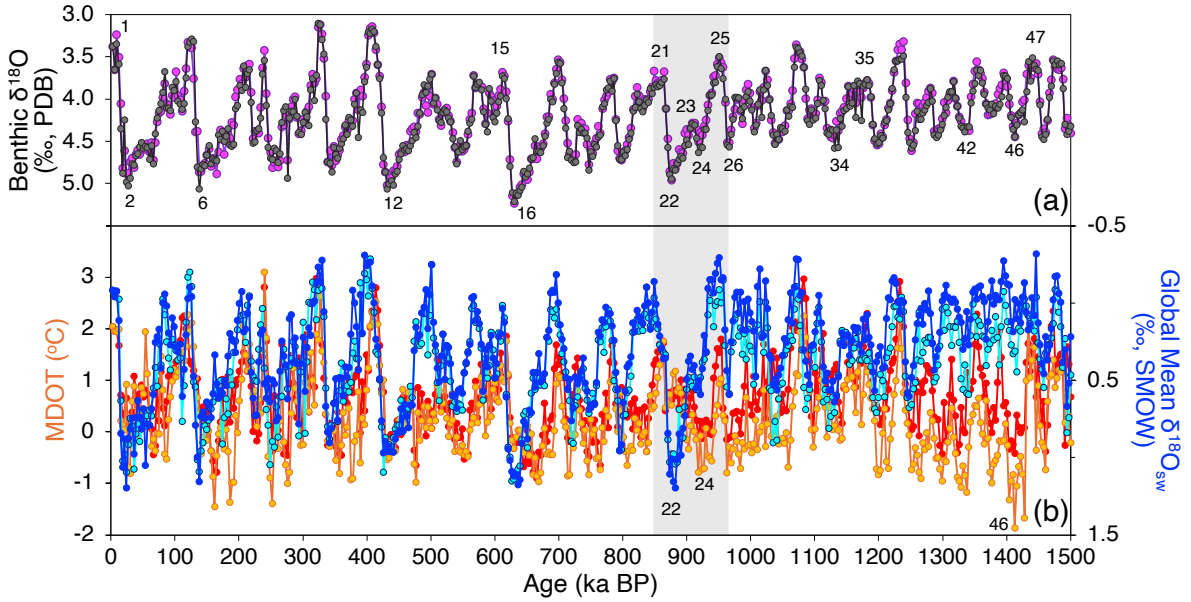


**Figure S10: Comparison of unweigted and volume-weighted global deep ocean stacks. (a) Unweighted (pink) and weighted (dark grey) benthic $\delta^{18}O$ with MIS numbers highlighting selected glacial (even) and interglacial (odd) stages. (b) Comparisons for global mean $\delta^{18}O_{seawater}$ between unweighted (light blue) versus volume-weighted (dark blue) stacks; and for MDOT between the unweighted (red) and volume-weighted (orange) stacks with the latter suggesting MIS 46 (~1420 ka) experienced the coldest deep-water temperatures of the last 1.5 Ma. The very low MDOTs during MIS 46 result from very low Mg/Ca ratio values that were not used (plotted) by Elderfield et al. (2012) because they suspected species/morphotype variations in Mg/Ca of *Uvigerina*. This does not seem to be borne out by a core-top study in the SW Pacific (Stirpe et al., 2021) and, hence, we didn't exclude them but they do result in suspiciously cold temperatures especially during MIS 46.**

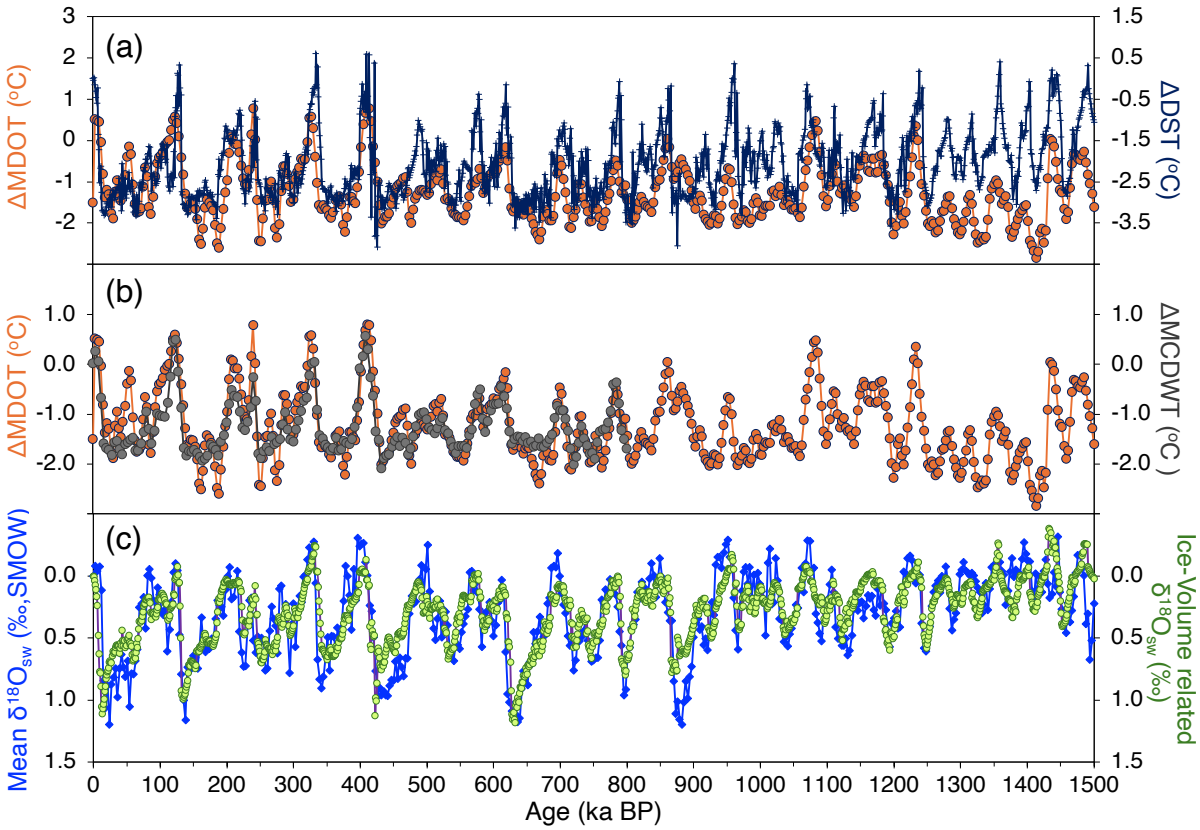

**Figure S11: Comparison of volume-weighted MDOT and mean $\delta^{18}O_{seawater}$ stacks against similar recently published estimates. (a) The change in smoothed, volume-weighted MDOT (ΔMDOT) (this study; orange line and circles) relative to an average present day value (1.5 ºC (Rohling et al., 2021, 2022)) versus the change in deep-sea temperature (ΔDST) estimated relative to the present (Rohling et al., 2021) (dark blue line with crosses) The two records are offset to each other by 1.5 ºC. (b) ΔMDOT as in (a) versus mean CDW temperature (ΔMCDWT) relative to present (Chandler and Langebroek, 2024) (dark grey line with markers). (c) Volume-weighted mean $\delta^{18}O_{seawater}$ stack (this study; blue line with diamonds) compared with process-based estimated ice-volume related deep-sea $\delta^{18}O_{seawater}$ (Rohling et al., 2021) (purple line with green circles).**

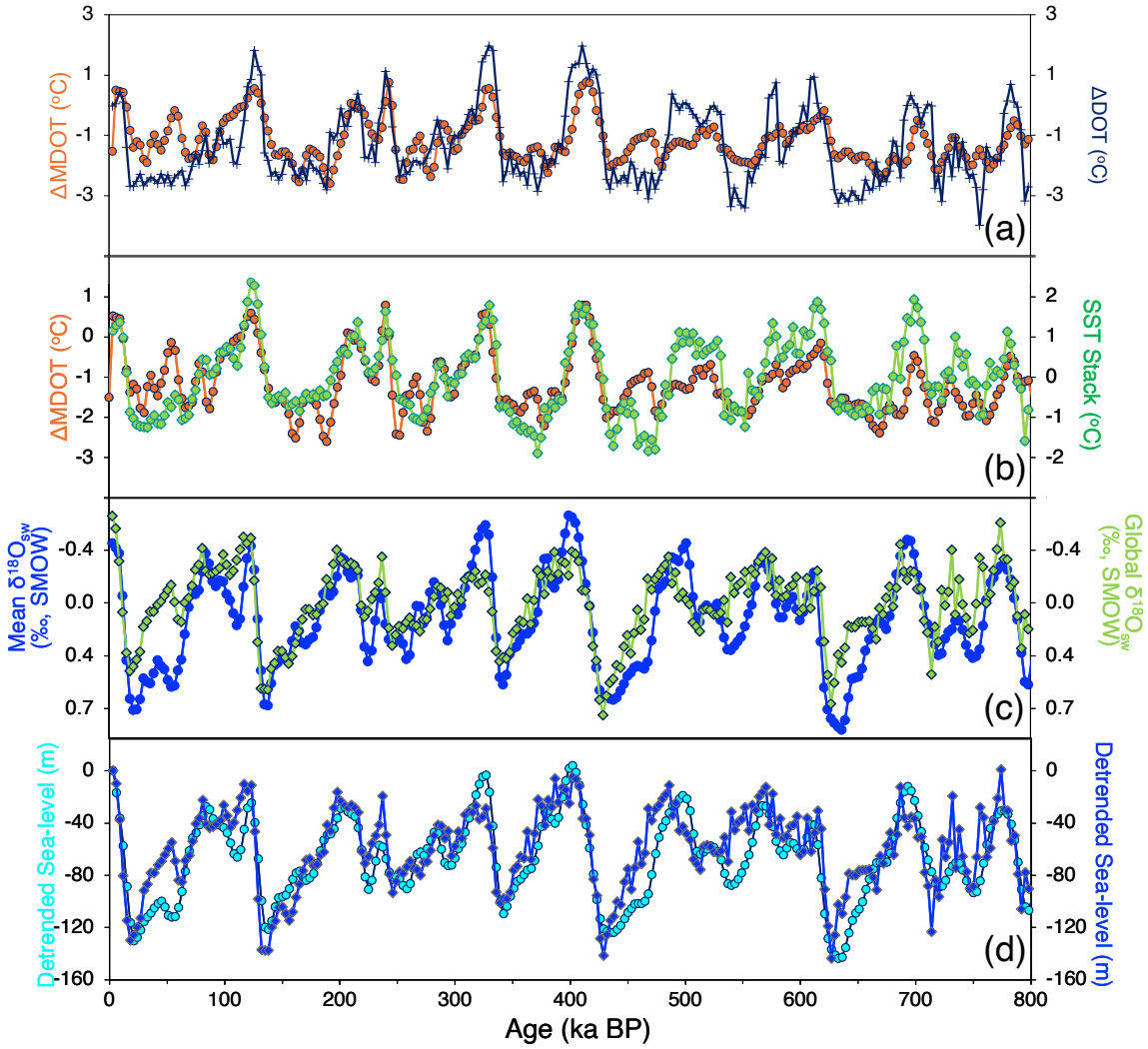


**Figure S12: Comparison of MDOT and mean $\delta^{18}O_{seawater}$ stacks against similar stacks derived from SST and paired planktonic $\delta^{18}O$. (a) and (b) Smoothed, volume-weighted MDOT (this study; orange line with circles) compared respectively to deep ocean (dark blue line with stars) and sea surface (green line and diamonds) temperature stacks (Shakun et al., 2015). (c) Smoothed, volume-weighted mean $\delta^{18}O_{seawater}$ (this study; dark blue line with circles) shifted to be centred at a mean of zero in line with the global $\delta^{18}O_{seawater}$ stack (Shakun et al., 2015) (green line with diamonds). (d) detrended sea-level whereby the smoothed, volume-weighted $\delta^{18}O_{seawater}$ record is converted to RSL using a two-point calibration formula ($y = \frac{y2-y1}{(x2-x1)} * (x - x1) + y1$ where x = measured $\delta^{18}O_{seawater}$, x1 = measured Holocene $\delta^{18}O_{seawater}$ value, x2 = measured Last Glacial Maximum (LGM) $\delta^{18}O_{seawater}$ value, and y1 and y2 are the Holocene and LGM values of 0 and -130 m respectively, following (Shakun et al., 2015)) (this study; blue line with light blue circles) versus detrended sea-level (Shakun et al., 2015) (dark blue line with diamonds).**

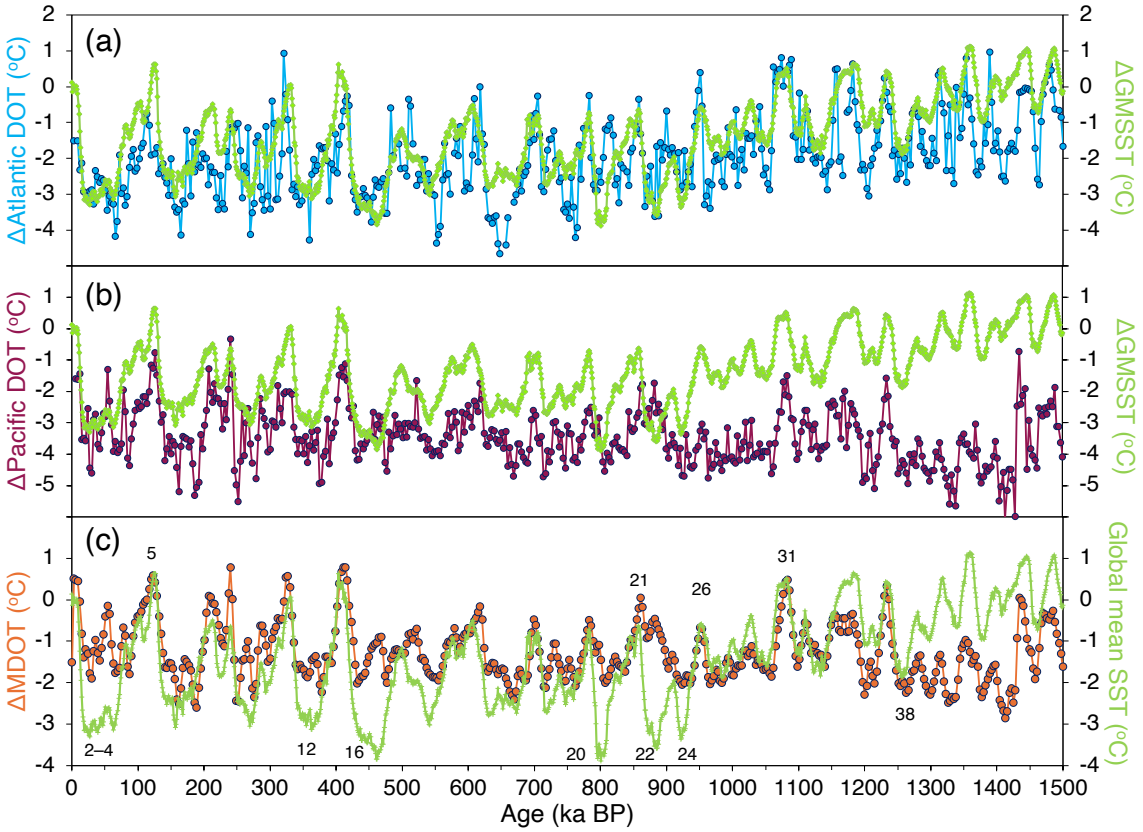


**Figure S13: Comparison of changes in Atlantic, Pacific, and mean deep ocean temperature stacks against changes in the stack of global mean SST. All panels show changes in the high-resolution area weighted global mean SST (ΔGMSST) stack referenced to the late Holocene (i.e. 0 °C at 0 ka) (Clark et al., 2024) (light green) versus changes in: (A) Atlantic deep ocean temperature (blue); (B) Pacific deep ocean temperature (dark red); and (C) Changes in smoothed, volume-weighted MDOT (ΔMDOT) (orange). Deep ocean temperatures are presented relative to an average present day value (1.5 °C (Rohling et al., 2021, 2022)). Numbers mark some important marine isotope stages.**

**Table S1: Analytical uncertainty in Mg/Ca records.**

| Site | Long-term standard error | Benthic Mg/Ca replicate error (mmol $mol^{-1}$) | Combined error (1σ) | 2σ Sigma error |
|---|---|---|---|---|
| IODP U1385: Uvig | 0.00598 | 0.092 | 0.093 | 0.185 |
| ODP 1123: Uvig | 0.00598 | 0.055 | 0.055 | 0.111 |
| DSDP 607: Uvig | 0.012 | 0.060 | 0.061 | 0.122 |
| DSDP 607: Cibs | 0.015 | 0.100 | 0.101 | 0.202 |
| ODP 1208: Uvig | 0.012 | 0.056 | 0.057 | 0.115 |
| ODP 1094: Mpomp | 0.00598 | 0.042 | 0.042 | 0.084 |

**Table S2: Ocean basin boundaries and volumes**

| | | | | | Basin Contribution to Stacks | | | |
|---|---|---|---|---|---|---|---|---|
| **Region** | **Depth Range** | **Latitude Range** | **Longitude Range** | **Volume (% global ocean)*** | **ALL (%) (n = 267)** | **NA & PO (%) (n = 215)** | **NA & SA (%) (n = 1)** | **PO & SA (%) (n = 11)** |
| Deep North Atlantic | 2000–5000 m | 0–65°N | 80°W-0° | 5.1 | 11.70 | 13.93 | 42.15 | |
| Deep South Atlantic | 2000–5000 m | 70°S–0 | 70°W-30°E | 7 | 16.06 | | 57.85 | 18.18 |
| Deep Pacific Ocean | 2000–5000 m | 70°S–55°N | 105°E-70°W | 31.5 | 72.25 | 86.07 | | 81.82 |
| Total global ocean represented (%) | | | | 43.6 | 43.6 | 36.6 | 12.10 | 38.50 |

*Note: to construct global weighted stacks, the percent volume for each basin is scaled to the sum of the regional volumes (i.e. 43.6 % when all three basins are represented). For example, the relative volume of the deep North Atlantic in this case is 5.1 / 43.6 = 11.7 %. In some cases, the entire value from a single basin is represented (Atlantic n = 2; Pacific n = 4). After (Lisiecki and Stern, 2016).

## References


Ahn, S., Khider, D., Lisiecki, L. E., and Lawrence, C. E.: A probabilistic Pliocene–Pleistocene stack of benthic $\delta^{18}O$ using a profile hidden Markov model, Dyn. Stat. Clim. Syst., 2, 1–16, https://doi.org/10.1093/climsys/dzx002, 2017.

Birner, B., Hodell, D. A., Tzedakis, P. C., and Skinner, L. C.: Similar millennial climate variability on the Iberian margin during two early Pleistocene glacials and MIS 3, Paleoceanography, 31, 203–217, https://doi.org/10.1002/2015PA002868, 2016.

Chandler, D. M. and Langebroek, P. M.: Glacial-interglacial Circumpolar Deep Water temperatures during the last 800,000 years: estimates from a synthesis of bottom water temperature reconstructions, Clim. Past, 20, 2055–2080, https://doi.org/10.5194/cp-20-2055-2024, 2024.

Clark, P. U., Shakun, J. D., Rosenthal, Y., Köhler, P., and Bartlein, P. J.: Global and regional temperature change over the past 4.5 million years, Science, 383, 884–890, https://doi.org/10.1126/science.adi1908, 2024.

Elderfield, H., Yu, J., Anand, P., Kiefer, T., and Nyland, B.: Calibrations for benthic foraminiferal Mg/Ca paleothermometry and the carbonate ion hypothesis, Earth Planet. Sci. Lett., 250, 633–649,

https://doi.org/10.1016/j.epsl.2006.07.041, 2006.
Elderfield, H., Greaves, M., Barker, S., Hall, I. R., Tripati, A., Ferretti, P., Crowhurst, S., Booth, L., and Daunt, C.: A record of bottom water temperature and seawater $\delta^{18}O$ for the Southern Ocean over the past 440 kyr based on Mg/Ca of benthic foraminiferal Uvigerina spp., Quat. Sci. Rev., 29, 160–169, https://doi.org/10.1016/j.quascirev.2009.07.013, 2010.
Elderfield, H., Ferretti, P., Greaves, M., Crowhurst, S., McCave, I. N., Hodell, D. A., and Piotrowski, A. M.: Evolution of ocean temperature and ice volume through the Mid-Pleistocene Climate Transition, Science, 337, 704–709, https://doi.org/10.1126/science.1221294, 2012.
Ford, H. L. and Raymo, M. E.: Regional and global signals in seawater $\delta^{18}O$ records across the mid-Pleistocene transition, Geology, 48, 113–117, https://doi.org/10.1130/G46546.1, 2020.
Ford, H. L., Sosdian, S. M., Rosenthal, Y., and Raymo, M. E.: Gradual and abrupt changes during the Mid-Pleistocene Transition, Quat. Sci. Rev., 148, 222–233, https://doi.org/10.1016/j.quascirev.2016.07.005, 2016.
Greaves, M. J.,: Trace elements in marine biogenic carbonates: Analysis and application to past ocean chemistry, Ph.D. thesis, University of Southampton 194 pp., 2008.
Hasenfratz, A. P., Martínez-García, A., Jaccard, S. L., Vance, D., Wälle, M., Greaves, M., and Haug, G. H.: Determination of the Mg/Mn ratio in foraminiferal coatings: An approach to correct Mg/Ca temperatures for Mn-rich contaminant phases, Earth Planet. Sci. Lett., 457, 335–347, https://doi.org/10.1016/j.epsl.2016.10.004, 2017.
Hasenfratz, A. P., Jaccard, S. L., Martínez-García, A., Sigman, D. M., Hodell, D. A., Vance, D., Bernasconi, S. M., Kleiven, H. (Kikki) F., Haumann, F. A., and Haug, G. H.: The residence time of Southern Ocean surface waters and the 100,000-year ice age cycle, Science, 363, 1080–1084, https://doi.org/10.1126/science.aat7067, 2019.
de Lange, G. J., van Os, B., and Poorter, R.: Geochemical composition and inferred accretion rates of sediments and managanese nodules from a submarine hill in the Madeira Abyssal Plain, eastern North Atlantic, Mar. Geol., 109, 171–194, https://doi.org/10.1016/0025-3227(92)90227-9, 1992.
Lisiecki, L. E. and Stern, J. V: Regional and global benthic $\delta^{18}O$ stacks for the last glacial cycle, Paleoceanography, 1368–1394, https://doi.org/10.1002/2016PA003002. 2016.
Martin, W. R. and Sayles, F. L.: $CaCO_3$ dissolution in sediments of the Ceara Rise, western equatorial Atlantic, Geochim. Cosmochim. Acta, 60, 243–263, https://doi.org/10.1016/0016-7037(95)00383-5, 1996.
Mashiotta, T. A., Lea, D. W., and Spero, H. J.: Glacial-interglacial changes in Subantarctic sea surface temperature and $\delta^{18}O$-water using foraminiferal Mg, Earth Planet. Sci. Lett., 170, 417–432, https://doi.org/10.1016/S0012-821X(99)00116-8, 1999.
Rohling, E. J., Yu, J., Heslop, D., Foster, G. L., Opdyke, B., and Roberts, A. P.: Sea level and deep-sea temperature reconstructions suggest quasi-stable states and critical transitions over the past 40 million years, Sci. Adv., 7, 1–17, https://doi.org/10.1126/sciadv.abf5326, 2021.
Rohling, E. J., Foster, G. L., Gernon, T. M., Grant, K. M., Heslop, D., Hibbert, F. D., Roberts, A. P., and Yu, J.: Comparison and synthesis of sea-level and deep-sea temperature variations over the past 40 million years, Rev. Geophys., 60, 1–56, https://doi.org/10.1029/2022rg000775, 2022.
Shakun, J. D., Lea, D. W., Lisiecki, L. E., and Raymo, M. E.: An 800-kyr record of global surface ocean $\delta^{18}O$ and implications for ice volume-temperature coupling, Earth Planet. Sci. Lett., 426, 58–68, https://doi.org/10.1016/j.epsl.2015.05.042, 2015.
Skinner, L. C. and Elderfield, H.: Rapid fluctuations in the deep North Atlantic heat budget during the last glacial period, Paleoceanography, 22, 1–9, https://doi.org/10.1029/2006PA001338, 2007.
Skinner, L. C., Shackleton, N. J., and Elderfield, H.: Millennial-scale variability of deep-water temperature and $\delta^{18}O_{dw}$ indicating deep-water source variations in the Northeast Atlantic, 0-34 cal. ka BP, Geochemistry, Geophys. Geosystems, 4, https://doi.org/10.1029/2003GC000585, 2003.
Sosdian, S. and Rosenthal, Y.: Deep-sea temperature and ice volume changes across the Pliocene-Pleistocene climate transitions, Science, 325, 306–310, https://doi.org/10.1126/science.1169938, 2009.
Stirpe, C. R., Allen, K. A., Sikes, E. L., Zhou, X., Rosenthal, Y., Cruz-Uribe, A. M., and Brooks, H. L.: The Mg/Ca proxy for temperature: A Uvigerina core-top study in the Southwest Pacific, Geochim. Cosmochim. Acta, 309, 299–312, https://doi.org/10.1016/j.gca.2021.06.015, 2021.
Weldeab, S., Arce, A., and Kasten, S.: Mg/Ca-$\Delta CO_3^{2-}{}_{\text{pore water}}$–temperature calibration for Globobulimina spp.: A sensitive paleothermometer for deep-sea temperature reconstruction, Earth Planet. Sci. Lett., 438, 95–102, https://doi.org/10.1016/j.epsl.2016.01.009, 2016.
Yu, J. and Broecker, Wallace, S.: Comment on "Deep-sea temperature and ice volume changes across the Pliocene-Pleistocene climate transitions," Science, 328, 1480, doi:10.1126/science.1186544, 2010.
Yu, J. and Elderfield, H.: Mg/Ca in the benthic foraminifera Cibicidoides wuellerstorfi and Cibicidoides mundulus: Temperature versus carbonate ion saturation, Earth Planet. Sci. Lett., 276, 129–139, https://doi.org/10.1016/j.epsl.2008.09.015, 2008.